

Available online at www.sciencedirect.com**ScienceDirect**

Geochimica et Cosmochimica Acta 173 (2016) 304–318

**Geochimica et
Cosmochimica
Acta**

www.elsevier.com/locate/gca

Lower mantle hydrogen partitioning between periclase and perovskite: A quantum chemical modelling

Marcello Merli ^a, Costanza Bonadiman ^b, Valeria Diella ^c, Alessandro Pavese ^{c,d,*}^a Department of Earth and Marine Sciences, University of Palermo, Via Archirafi 36, 90123 Palermo, Italy^b Department of Physics and Earth Sciences, University of Ferrara, Via Saragat 1, 44122 Ferrara, Italy^c Consiglio Nazionale delle Ricerche, CNR-IDPA, Section of Milan, Via Mangiagalli 34, 20133 Milan, Italy^d Department of Earth Sciences “A. Desio”, University of Milan, Via Botticelli 23, 20133 Milan, Italy

Received 2 April 2015; accepted in revised form 27 October 2015; available online 6 November 2015

Abstract

Partitioning of hydrogen (often referred to as H₂O) between periclase (*pe*) and perovskite (*pvk*) at lower mantle conditions (24–80 GPa) was investigated using quantum mechanics, equilibrium reaction thermodynamics and by monitoring two H-incorporation models. One of these (MSWV) was based on replacements provided by Mg²⁺ ↔ 2H⁺ and Si⁴⁺ ↔ 4H⁺; while the other (MSWA) relied upon substitutions in 2Mg²⁺ ↔ Al³⁺ + H⁺ and Si⁴⁺ ↔ Al³⁺ + H⁺. H₂O partitioning in these phases was considered in the light of homogeneous (Bulk Silicate Earth; *pvk*: 75%–*pe*:16% modal contents) and heterogeneous (Layered Mantle; *pvk*:78%–*pe*:14% modal contents) mantle geochemical models, which were configured for lower and upper bulk water contents (*BWC*) at 800 and 1500 ppm, respectively. The equilibrium constant, *BWC*K(*P,T*), for the reactions controlling the H-exchange between *pe* and *pvk* exhibited an almost negligible dependence on *P*, whereas it was remarkably sensitive to *T*, *BWC* and the hydrogen incorporation scheme. Both MSWV and MSWA lead to *BWC*K(*P,T*) ≤ 1, which suggests a ubiquitous shift in the exchange reaction towards an H₂O-hosting perovskite. This took place more markedly in the latter incorporation mechanism, indicating that H₂O-partitioning is affected by the uptake mechanism. In general, the larger the *BWC*, the smaller the *BWC*K(*P,T*). Over the *BWC* reference range, MSWV led to *BWC*K(*P,T*)-grand average ($\langle BWC \rangle$) calculated along lower mantle *P-T*-paths of ≈0.875. With regard to the MSWA mechanism, $\langle BWC \rangle$ was more sensitive to *BWC* (and LM over BSE), but its values remained within the rather narrow 0.61–0.78 range. The periclase–perovskite H₂O concentration-based partition coefficient, Kd_{H₂O}^{pe/pvk}, was inferred using $\langle BWC \rangle$, assuming both hydrous and anhydrous-dominated systems. MSWV revealed a Kd_{H₂O}^{pe/pvk}–*BWC* linear interpolation slope which was close to 0 and Kd_{H₂O}^{pe/pvk} values of 0.36 and 0.56 (for anhydrous and hydrous system, respectively). MSWA, in turn, yielded a Kd_{H₂O}^{pe/pvk} trend with a slightly steeper negative *BWC*-slope, while it may also be considered nearly invariant with Kd_{H₂O}^{pe/pvk} values of 0.31–0.47 in the 800–1500 ppm interval. Combining the MSWV and MSWA results led to the supposition that Kd_{H₂O}^{pe/pvk} lies in the narrow 0.31–0.56 interval, as far as the *P-T-BWC* values of interest are concerned. This implies that water always prefers *pvk* to *pe*. Furthermore, it also suggests that even in lower mantle with low or very low bulk water content, periclase rarely becomes a pure anhydrous phase.

© 2015 Elsevier Ltd. All rights reserved.

1. INTRODUCTION

* Corresponding author at: Department of Earth Sciences “A. Desio”, University of Milan, Via Botticelli 23, 20133 Milan, Italy.
Tel.: +39 02 503 15603.

E-mail address: alessandro.pavese@unimi.it (A. Pavese).

Hydrogen incorporation mechanisms in nominally anhydrous minerals (NAM) control the “water” exchange (this term, along with H₂O, is here used to refer to the H-content

of a mineral, expressed in terms of oxides) between the Earth's interior and its surface, as well as the degree of retention and potential abundance of hydrogen deep inside our planet (Ahrens, 1989; Smyth, 2006; Johnson, 2006; Hirschmann, 2006; Hirschmann and Kohlstedt, 2012).

Metal-silicate partitioning experiments (Li and Agee, 1996; Abe et al., 2000; Saxena et al., 2004; McDonough and Arevalo, 2008) seem to suggest that the Earth's core may contain water, although the volatile species geochemical model (Marty, 2012) does not support the notion that H_2O could have been stored there during accretion and terrestrial differentiation processes.

Water mass estimates in the main mineral phases of our planet's interiors (i.e. Murakami et al., 2002; Ohtani, 2005; Inoue et al., 2010), combined with geochemical bulk models (i.e. McDonough and Sun, 1995; Lyubetskaya and Korenaga, 2007; Wood and Corgne, 2007; Javoy et al., 2010), suggest that the Earth's mantle may host between 0.5 and 5 oceans (Huang et al., 2005; Smyth and Jacobsen, 2006; Khan and Shankland, 2012; Marty, 2012).

Bulk Silicate Earth chemical models indicate that MgO and FeO provide over 50% oxide weights (e.g. McDonough and Sun, 1995; Palme and O'Neill, 2003; Lyubetskaya and Korenaga, 2007; Javoy et al., 2010), with olivine (and its high pressure β - and γ -polymorphs) being the dominant mineral in the upper mantle. Olivine incorporates hydrogen *via* intrinsic point defects in its structure (Ingrin and Skogby, 2000; Bolfan-Casanova, 2005; Hauri et al., 2006), amounting to nearly the equivalent volume of Earth's oceans (Hirschmann et al., 2005, 2009; Khan and Shankland, 2012).

The water content incorporated by NAMs in the transition zone (410–660 km depth) is larger by as much as an order of magnitude (Bolfan-Casanova, 2005; Khan and Shankland, 2012) than that stored in the shallow upper mantle (Hirschmann et al., 2005; Bonadiman et al., 2009; Inoue et al., 2010). Recently, evidence provided by ring-woodite inclusions in diamond indicated that the transition zone is at least locally hydrated (Pearson et al., 2014), accommodating up to 3.3 wt% water (Smyth, 1994; Bolfan-Casanova et al., 2000; Kleppe, 2006; Griffin et al., 2013), and represents a potential hydrogen reservoir that might store up to approximately four times the water in oceans and atmosphere (Hirschmann, 2006; Dai and Karato, 2009; Griffin et al., 2013).

The precise amount of stored water in the lower mantle, its location and the mechanisms of its exchange with the upper mantle are still a matter of debate (e.g. Hirschmann et al., 2005; Bolfan-Casanova et al., 2006; Panero et al., 2015). In such a region, silicate Mg -perovskite and Fe -periclase are the principal mineral phases (Guyot et al., 1988; Ito and Takahashi, 1989; Ringwood, 1991; Fiquet et al., 1998). Experimental studies (Bolfan-Casanova et al., 2000; Murakami et al., 2002; Litasov and Ohtani, 2007; Joachim et al., 2013) suggest that the partitioning coefficient for hydrogen between $(Mg, Fe)O$ and $(Mg, Fe)(Si, Al)O_3$ is >1 at 23–25 GPa and 1675–2275 K, with H_2O -contents in periclase ranging from 40–60 to 2000 ppm (Bolfan-Casanova et al., 2000; Murakami et al., 2002). However, Hernández et al. (2013) predicted that in Fe -free environment and at 24 GPa and 1500 K, water tends to be incorporated into

perovskite rather than periclase. Although extensive investigations (e.g. Mosenfelder et al., 2013; Jahn et al., 2013; Ghosh et al., 2013) have been devoted to hydrogen incorporation, there is much uncertainty about the microscopic mechanisms underlying such reactions. In literature, several models are available to account for the uptake of hydrogen in high-pressure mineral phases: cation-vacancy occurrence and H-compensation (hydro-garnet-like substitution); double replacement, such as $2Mg/1Si \leftrightarrow Al(Fe^{3+}) + H$; reduction of iron to Fe -metallic (Keppler and Bolfan-Casanova, 2006; Litasov, 2010).

Although little is known about water solubility in periclase and perovskite at lower mantle pressure, it is reasonable to say that the pure H_2O - MgO - SiO_2 system is probably a weak acceptor and most H-incorporation is related to double-replacement mechanisms involving mainly aluminium and ferric iron (McCammon et al., 2004; Panero and Stixrude, 2004). Demouchy et al. (2007) and Mackwell et al. (2005) discussed the role of ferric iron in combination with vacancy occurrence (at hydrous-ambient-pressure conditions), whereas Bolfan-Casanova et al. (2006) observed that at high pressure, Fe anti-correlates with hydroxyl formation. In particular, Fe -periclase and perovskite can host heterovalent cations through coupled substitutions as well as the creation of point defects (Van Orman et al., 2009) over a wide $P-T$ range. Fe^{3+} dwelling in $(Mg, Fe)O$ (i.e. McCammon et al., 2004; Otsuka et al., 2010; Lin and Wheat, 2012) shows pressure/oxygen fugacity dependence, so that in the lower mantle a change in the crystal-chemical behaviour of ferric iron is expected (Otsuka et al., 2010). On the basis of experimental and theoretical data, it is plausible to assume that $(Mg, Fe)O$ in the shallow part of the lower mantle ($P \approx 25$ –28 GPa) hosts Fe^{3+} in octahedral sites, in combination with cation vacancies or the occurrence of a monovalent cation (Na^+) in order to fulfil charge balance. Solubility competition between monovalent cation (Na^+) and protons (H^+) may play a role in the tendency of H to site in periclase or perovskite in the deep region of the lower mantle (McCammon et al., 2004).

Seismological heterogeneities and tomographic models at the core-mantle boundary (i.e. 2300–2800 km depth) reveal (Hilst et al., 1997; Lay et al., 1998; Wysession et al., 1998; Garnero et al., 2004; Nomura et al., 2014) a distinct layer (D'' ; Kellogg et al., 1999; Montelli et al., 2004; Wolfe et al., 2009), possibly due to changes in the iron chemistry and Mg/Fe ratio related to phase transitions (Kellogg et al., 1999; Mao et al., 2006). The potential segregation of even a small amount of water in this region, or in the Earth's core, could drastically modify both melting relationships (e.g., Inoue, 1994; Lay et al., 2004; Saxena et al., 2004) and rheological properties (e.g., Mei and Kohlstedt, 2000; Karato and Jung, 2003), thus ultimately affecting dynamics and evolution modelling in terrestrial planets.

From this view point, quantum mechanical modelling and computing techniques are able to provide a valuable way of complementing experimental data, by substantiating existing hypotheses or contributing to the development of new ones. The aim of the present work was twofold: (1) to use quantum mechanics [HF/DFT-LCAO calculations; CRYSTAL09-program (Dovesi et al., 2009)] to model the

equilibrium constant, $K(P, T)$, for reactions involving water exchange between periclase (*pe*) and perovskite (*pvk*) at lower mantle regime by adopting two H-incorporation schemes; (2) to exploit the theoretical results in order to predict hydration/dehydration trends and potential H_2O -distribution between *pe* and *pvk* in the light of lower mantle geochemical models.

2. GEOCHEMICAL CONSTRAINTS

Solid–solid H_2O partitioning in the lower mantle ultimately depends on which Bulk Earth geochemical model is used to account for the lower mantle whole chemical composition.

Two distinct lower mantle geochemical models were considered:

- 1) The homogeneous mantle model (BSE = Bulk Silicate Earth), which is inferred from the Primitive Upper Mantle (PUM) composition according to terrestrial data (pyrolite) and chondritic constraints (e.g. McDonough and Sun, 1995; Zindler and Hart, 1986; Lyubetskaya and Korenaga, 2007; Javoy et al., 2010), and it is extended to the whole silicate Earth;
- 2) The heterogeneous mantle model (LM = layered mantle), which is based on geophysical data and cosmochemical constraints; it proposes a lower mantle which is chemically distinct from the upper mantle (e.g. Anderson, 1989; Stixrude and Bukowinski, 1992; Cammarano and Romanowicz, 2007; Matas et al., 2007; Javoy et al., 2010). In order to match the cosmochemical major element contents of the bulk mantle (Matas et al., 2007), the LM lower mantle must have higher Si content than PUM ($Mg/Si_{PUM} = 1.21\text{--}1.31$; $Mg/Si_{LM} = 1.18$, Table 1).

Lower mantle mineral phase composition, which depends upon which geochemical model has been chosen, stems from mass balance calculations, aimed at giving the best fit for expected mineral phases and the overall rock composition (Table 1). $CaSiO_3$ –perovskite occurs along with $(Mg, Fe)SiO_3$ –perovskite and $(Mg, Fe)O$ –periclase. Although Al_2O_3 oxide accounts for about 3.5–4.5 wt% of the lower mantle, the aluminium host-phase is still uncertain. Al may reside in $(Mg, Fe)O$ –*pe* and $(Mg, Fe)SiO_3$ –*pvk* (Irifune, 1994; Irifune et al., 1996), or form a separate Al-rich phase (Kesson et al., 1995; Oganov and Brodholt, 2000; Pamato et al., 2015). In Table 1, Al_2O_3 was assumed to be associated to a “nondescript” HP-phase, which corresponds to 2–3 wt% of the lower mantle modal composition (see Ohira et al., 2014, regarding Al-bearing δ -phase stability). Preliminary mass balance tests suggested SiO_2 –stishovite exclusion. Lower mantle H_2O content was estimated by subtracting upper mantle and transition zone contributions, normalised to their respective fractional masses (Table 2) from the Bulk Mantle. Note that Bulk Mantle shares H_2O content with BSE, excluding surface water reservoirs (atmosphere, oceans and sedimentary rocks) and adopting normalisation to the total Earth mass, as proposed by Marty (2012).

Table 1

Lower mantle major element composition and mineral modal estimates obtained by mass balance calculations.

	BSE	LM		
	*	**	#	***
wt%				
SiO_2	45.00	45.01	47.53	
Al_2O_3	4.45	3.59	4.04	
FeO	8.05	7.94	8.23	
MgO	37.80	38.97	37.87	
CaO	3.55	2.73	2.32	
Mg – <i>Pvk</i>	74	76	75	78
<i>Pe</i>	16	16	16	14
Ca – <i>Pvk</i>	7	6	6	6
Al_2O_3 –HPphase	3	2	3	2
	$r^2 = 0.34$	$r^2 = 0.13$		$r^2 = 0.41$

The lower mantle mineral phase compositions which were used to calculate the mass balance are taken from Walter et al. (2004) and Corrige et al. (2005). BSE = Bulk Silicate Earth; LM = layered mantle. Mg –*Pvk* = magnesium–perovskite; *Pe* = periclase; Ca –*Pvk* = calcium–perovskite ; Al_2O_3 –HPphase = High Pressure Aluminium Phase.

* McDonough and Sun (1995).

** Javoy et al. (2010).

*** After Matas et al. (2007).

Averaged mineral modal percentage used for BSE in this work.

H_2O global estimates converge at 250 ± 50 ppm for the upper mantle (Michael, 1988; Dixon et al., 2002; Saal et al., 2002; Salters and Stracke, 2004) and 1.0 ± 0.3 wt% for the transition zone (Ohtani, 2005; Pearson et al., 2014). Lower mantle minimum/maximum Bulk Water Content (hereafter *BWC*; Table 2) figures were inferred to be smaller than 1000 and 2000 ppm, respectively, using a conservative H_2O estimate in line with BSE (1100–3000 ppm; Palme and O’Neill, 2003; Ohtani, 2005; Marty, 2012), and combining it with the mantle mass fractions (Table 2). The resulting *BWC* estimates are in agreement with earlier studies (Murakami et al., 2002; Ohtani, 2005; Hernández et al., 2013). For this reason, 800 and 1500 ppm reference average values were chosen as lower and upper *BWC* estimates, respectively; precise values depend on the geochemical model and will be considered below, in the Section 8.

3. H-INCORPORATION MODELLING

Two mechanisms were considered in order to account for H-incorporation in *pe* and *pvk*, at lower mantle conditions (Kröger–Vink formalism; Kröger, 1972):

MSWV-scheme (Magnesium, Silicon, Water, Vacancies), relying upon

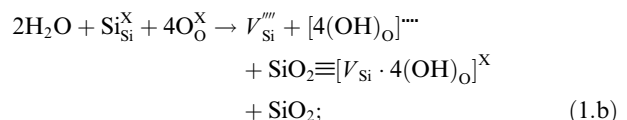
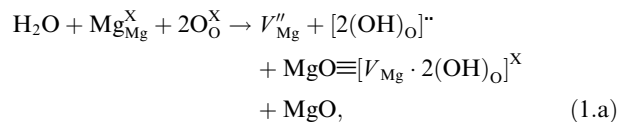


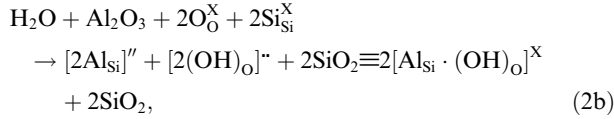
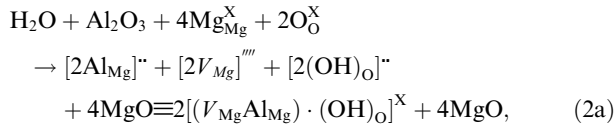
Table 2
Water budget estimates in mantle repositories.

Earth mass (g)	BSE mass (g)	Upper mantle	Transition zone	Lower mantle	Bulk mantle
		(Fraction of Earth total mass)			
5.98E+27	4.00E+27	0.103	0.075	0.492	
Thickness (km)		420	300	2170	2890
H ₂ O (ppm)	1100–3000 ^{1,2,3}	200–300 ^{4,5}	1.0–1.3 (wt%) ^{6, 7}	A-2000 ^{6,8,9} 800/1500 ^(this study)	1500–2400 ^{3,6}
Suggested value		250	1.2 (wt%)		(A: value < 1000 ppm).

1 = McDonough and Sun (1995); 2 = Palme and O'Neill (2003); 3 = Marty (2012); 4 = Dixon et al. (2002); 5 = Saal et al. (2002); 6 = Ohtani (2005); 7 = Pearson et al. (2014); 8 = Murakami et al. (2002); 9 = Hernández et al. (2013).

Bold values: reference average values for lower and upper Bulk Water Contents respectively used for calculation.

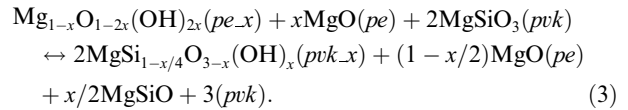
MSWA-scheme (Magnesium, Silicon, Water, Aluminium), based on



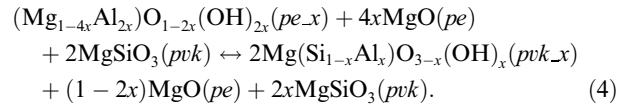
where vacancies and substitutions are defined in terms of replaced species (subscript) and excess charge (superscript), which can be neutral (X), positive (•) or negative ('). Hydrogen is referred to as a hydroxyl-group replacing an oxygen and is written as (OH)_O. Other possible H-incorporation mechanisms which were similar to those detailed above but use Fe³⁺ were neglected as attention was focused on partitioning reactions controlled by sub-solidus atomic replacements, thus excluding those that also involve environmental redox-conditions. In Eqs. (1.a) and (1.b), incorporation via replacement of one Mg/Si with 2/4 H atoms was assumed. Such a scheme may lead to the formation of (i) hydroxyl groups (Smyth, 2006; Panero et al., 2015) which are shaped by incorporated H and coordination oxygens, and (ii) X-cation vacancies (V_X) at the expenses of either magnesium (in pe) or silicon (in pvk). In pvk, the substitution of one sixfold coordinated Si with four H atoms, which likely form as many hydroxyl groups with vertex oxygens in the same polyhedron, accounts for an analogous replacement taking place in hydro-garnet, although in this case relating to tetrahedrally coordinated silicon (Williams and Hamley, 2001). The substitution of one Mg versus two hydrogen atoms in pvk has recently been explored (Hernández et al., 2013), providing a pe/pvk-partition coefficient for H of ≈0.01. The present study complements this research in terms of Si-involving mechanisms for H incorporation. In Eqs. (2.a) and (2.b), H enters pe and pvk, along with Al, to replace two Mg atoms and one Si atom, respectively. The sites vacated by Mg/Si host Al, whereas H establishes hydroxyls with coordination oxygens.

The leading reaction schemes at equilibrium for x-moles of H₂O entering either pe (1 mol) or pvk (2 mol), are in agreement with the average phase molar proportions determined by lower mantle models (Table 1). x-H₂O is often

referred to as “H/H₂O-uptake” or “H/H₂O-exchange”. According to the MSWV scheme, the equation below holds



MSWA, which in turn is likely to be closer to the physical uptake mechanism and requires an additional x-molar content of Al₂O₃, is associated with the equilibrium reaction shown below:



pe_x and pvk_x refer to H-bearing periclase and perovskite, with compositions according to the above equations. Note that a hydroxyl-based notation was used in order to stress possible OH formation, as stated above.

4. EQUILIBRIUM CONSTANT

At equilibrium, the reactions described by Eq. (3) and (4) require that

$$\Phi_{pe}\mu(pe) + \Phi_{pe_x}\mu(pe_x) + \Phi_{pvk}\mu(pvk) = \Omega_{pe}\mu(pe) + \Omega_{pvk_x}\mu(pvk_x) + \Omega_{pvk}\mu(pvk) \quad (5.a)$$

or

$$\sum_k \Phi_k \mu(k) = \sum_j \Omega_j \mu(j) \quad (5.b)$$

where $\mu(k)$ is the chemical potential associated with the kth-component and depends on P, T and component-molar-contents; Φ_k and Ω_j are the coefficients which provide the proportions for the substances in left- and right-hand members, respectively, in the equations above.

Moreover,

$$\mu(k) = \mu_0(k) + RT \ln(a_k), \quad (5.c)$$

where R is gas constant, $\mu_0(k)$ depends on P and T only, and a_k is activity. The equilibrium constant $K(P, T, x)$ for the reactions under study can be expressed as

$$K(P, T, x) = \left[\frac{\prod_k a_k^{\Phi(k)}}{\prod_j a_j^{\Omega(j)}} \right] = \exp(-\Delta G_0(P, T, x)/RT) \quad (6.a)$$

where:

$$\begin{aligned}\Delta G_0(P, T, x) = & \Phi_{pe_x} \mu_0(pe_x) - \Omega_{pvk_x} \mu_0(pvk_x) \\ & + (\Phi_{pe} - \Omega_{pe}) \mu_0(pe) + (\Phi_{pvk} \\ & - \Omega_{pvk}) \mu_0(pvk)\end{aligned}\quad (6.b)$$

The dependence of $\Delta G_0(P, T, x)$ on T was estimated via harmonic lattice dynamics modelling and semi-empirical potentials (Gale, 1997). At high-pressure, the effect of the part of $\Delta G_0(P, T, x)$ which is dependent on atomic vibrations was seen to be insignificant compared to that due to static contributions.

Pressure, in turn, was determined as $P = -\partial F(V, T)/\partial V$, by calculating static and vibrational energy contributions using quantum-mechanics and semi-empirical potentials, respectively, for pure periclase and perovskite. The correction due to the vibration contribution of Helmholtz free-energy (zero-point-motion and thermal pressure) ranges from 6 to 10 GPa, approximately, over the T -interval of interest. Anharmonic effects are negligible for two reasons:

- (i) calculations proved harmonic contributions to be insignificant. Therefore, the anharmonic part representing a higher order of approximation is negligible;
- (ii) in general, apart from some particular cases such as Ca-perovskite (Stixrude et al., 2007), anharmonicity loses impact at high-pressure (Stacey and Isaak, 2003; Wentzcovitch et al., 2010).

5. COMPUTING

Ab-initio Linear-Combination-of-Atomic-Orbital calculations (HF/DFT-CRYSTAL09 program; Dovesi et al., 2009) were carried out for pe_x and pvk_x , over a pressure range of 24–80 GPa. This P interval is so wide as to broadly encompass that of “pyrolite” liquidus (i.e. Corgne et al., 2005) at lower mantle pressures, inferred from the melting experiments of Trønnes and Frost (2002) and Ito et al. (2004). At $P > 24$ GPa, the sub-solidus post-spinel transition is completed even in the presence of 2 wt.% H₂O (Ghosh et al., 2013); setting an upper P -limit of 80 GPa (~ 2000 km depth) allows the D” region to be excluded, where the developed mineral partitioning model cannot be used.

Periclase and perovskite structures were relaxed to equilibrium at a given nominal pressure and 0 K; the former was then corrected to account for zero-point-motion and thermal pressure. The computing set-up (i.e. tolerances governing the accuracy of the integrals; SCF-cycle convergence parameters; k -sampling) used by Merli et al. (2015) was applied; for this reason, only the most relevant aspects are reported here. A Hamiltonian was adopted, based on the WC1LYP scheme (Scanaiano et al., 2012; Scanaiano and Prencipe, 2013), which contains a hybrid Hartree–Fock/density functional exchange–correlation term that mixes the WCGGA exchange component (Wu and Cohen, 2006) with the exact nonlocal HF exchange contribution and models the correlation energy via the Lee–Yang–Parr GGA

functional (Lee et al., 1988). In the case of pe , a hybridization rate (HR) of 20% was used (calculated versus observed energy-band-gap: 7.2 and 7.2/7.7 eV; Cappellini et al., 2000; Zhao and Truhlar, 2009), whereas HR was set at 28% for pvk (calculated versus other DFT-theoretical estimates of the energy-band-gap: 9.1 and 6.2 eV; Stashan et al., 2009). Such values proved to correctly model the equation of state, geometry and phase transition pressures (Parisi et al., 2012). Ten $H(P)$ -values were sampled for perovskite, using 20% HR over the chosen P -interval, in order to assess the effect of the energy-shift due to different HR-ratios. The enthalpy differences, compared to those with 28% HR, affect the equilibrium constants and the inferred concentration ratios by 3–12%, a negligible figure, in view of the degree of approximation for such a complex process. Thus, no significant shift of the equilibrium in the reactions (3) and (4) was caused. Water dissolution in pe and pvk was modelled on super-cells (up to 64 and 108 octahedral sites, for MgO and MgSiO₃, respectively, corresponding to 32 and 27 primitive cells) where the replacements (1.a) and (1.b) and (2.a and 2.b) mimic H incorporation. The super-cell size was tuned in order to enable different degrees of water dilution to be reproduced in the crystal structures by introducing one defect at a time. A fully linear enthalpy trend as a function of H-content was observed, which reinforced the physical soundness of the incorporation modelling scheme used.

The start Gaussian LCAO basis set of Mg was taken from Causà et al. (1986), then improved by adding diffuse sp and d shells so as to obtain an 85-11G* contraction. For O, the basis set of Ottonello et al. (2008) was used and extended by a d shell to get an 84-11G* contraction. In the case of Fe, the basis set of Valerio et al. (1995) was adopted, corresponding to an 86-41G* contraction scheme. A variational re-optimisation of the exponents of the most diffuse Gaussian functions of all three elements was also tested in pe and pvk , with no significant enhancement compared to the original values (see Belmonte et al., 2013, 2014 regarding the use of optimised basis sets compared to those in the present work). Further calculations were carried out by semi-empirical potentials and lattice dynamics using the GULP code, in order to estimate the effect of the vibration contribution on $\Delta G_0(P, T, x)$, as stated in the previous section. Mg–O, Si–O, O–O and H-involving interactions were modelled using Buckingham-type potentials from the program repository (Gale, 1997; Litton and Stephen Garofalini, 2001). Merli et al. (2015) provided details on the ability of such a potential to reproduce specific heat at constant volume, i.e. $C_V(T)$, and entropy for MgO. This data, complemented with calculations for perovskite, are here reported. In the case of MgO, the quoted authors report an agreement of 0.3% and 10% between theoretical calculations and experimental data for $C_V(T)$ over the explored thermal range and S^{298K} , respectively. Discrepancies of 1.6 and 26% for $C_V(T)$ and S^{298K} , respectively, were observed using experimental data from Anderson (1998) for perovskite, over the 400–1800 K range.

6. $K(P,T,X)$ CALCULATION

The equation

$$\mu_0(A_x, P, T) = H_0(A_x, P) - T \times S(A_x)_{\text{config}}, \quad (7)$$

can now be considered, where $H_0(A_x, P)$ and $S(A_x)_{\text{config}}$ are the enthalpy and configuration entropy, due to cation order-disorder, in the A_x phase, taking into account that energy calculations were restricted to static contributions only. A first order expansion in x suffices to provide the correct description of enthalpy as substantiated by trends of $H_0(A_x, P)$ for pe_x and pvk_x , determined by exploring 80 P - x points systematically sampled over the 20–80 GPa and 0–0.02 range for both phases. Linear interpolations in x of points sharing the same P yield R -values which are greater than 0.999, so that $H_0(A_x, P) \approx H_0(A, P) + \omega(A, P) \times x$, where ω depends on the incorporation scheme. Altogether, Eq. (6.b) for MSWV results in

$$\begin{aligned} \Delta G_0(P, T, x) = & \{[\omega_{\text{MSWV}}(pe, P) - 2 \times \omega_{\text{MSWV}}(pvk, P)] \\ & + 0.5 \times [3 \times H_0(pe, P) \\ & - H_0(pvk, P)]\} \times x - T \\ & \times \Delta S(x)_{\text{MSWV, config}} \end{aligned} \quad (8.a)$$

and

$$\begin{aligned} \Delta S(x)_{\text{MSWV, config}} = & R \times [x/2 \times \ln(4/3) + 1/2 \times x \times \ln(x) \\ & + (1-x) \times \ln(1-x) - 2 \times (1-x/4) \\ & \times \ln(1-x/4)]. \end{aligned}$$

For MSWA:

$$\begin{aligned} \Delta G_0(P, T, x) = & \{[\omega_{\text{MSWA}}(pe, P) - 2 \\ & \times \omega_{\text{MSWA}}(pvk, P)] + 2.0 \times [3 \\ & \times H_0(pe, P) - H_0(pvk, P)]\} \times x - T \\ & \times \Delta S(x)_{\text{MSWA, config}} \end{aligned} \quad (8.b)$$

and

$$\Delta S(x)_{\text{MSWA, config}} = R \times [2 \times x \times \ln(3/2) + (1-2 \times x) \\ \times \ln(1-2 \times x) - 2 \times (1-x) \times \ln(1-x)].$$

Moreover, it can be observed that

$$\begin{aligned} \xi_{0,x} &= 3 \times H_{0,x}(pe, P) - H_{0,x}(pvk, P) \\ &= a_{0,x} + a_{1,x} \times P + a_{2,x} \times P^2 \end{aligned} \quad (9.a)$$

and

$$\begin{aligned} \xi_{\omega,x} &= \omega_x(pe, P) - 2 \times \omega_x(pvk, P) \\ &= \omega_{0,x} + \omega_{1,x} \times P + \omega_{2,x} \times P^2, \end{aligned} \quad (9.b)$$

so that

$$\begin{aligned} \Delta G_{0,x}(P, T, x) &= (C \times \xi_{0,x} + \xi_{\omega,x}) \times x - T \\ &\quad \times \Delta S(x)_{X,\text{config}} \\ &= (\xi''_{0,x} + \xi_{\omega,x}) \times x - T \\ &\quad \times \Delta S(x)_{X,\text{config}} \end{aligned} \quad (10)$$

where the subscript X stands for either MSWV or MSWA; C is set at 0.5, for MSWV, and at 2, for MSWA.

The a_k/ω_j -parameters, referred to in Eqs. (9.a) and (9.b), are reported in Table 3, as calculated for the MSWV and MSVA models. It is worth noting that if $x\text{-H}_2\text{O}$ is assumed to be exchanged between partially hydrogenated perovskite and periclase, in contrast to the present model which relies on initially anhydrous H-exchangers, $K(P, T, x)$ would only be slightly affected compared to the value of the calculations reported here.

7. RESULTS

H and Al positions were determined using the least-enthalpy principle for either incorporation schemes, by exploring all possible H *versus* O configurations and taking into account the principle of local charge balance. In particular, it was assumed that H locates close to one of the corner-oxygen atoms of an octahedron which has been vacated by Mg/Si. Arrangements of H around O were explored, starting from hydrogen and oxygen 1.5–2.0 Å apart, for each possible octahedral H-configuration. Such calculations, performed at 40 GPa on least-enthalpy relaxed structures, provided approximate hydrogen positions, which were then used as initial suppositions over the investigated P -range. Note that the formation of hydroxyl-groups occurred, as suggested by the hydrogen–oxygen distances, which range from 0.97 to 1.06 Å. Fig. 1a–d provide examples of H-involving structure arrangements. According to MSWV, H atoms lie along, or are slightly oblique to, one of the main diagonals of the Si/Mg-emptied octahedron, pointing towards the vacant site and establish hydroxyl groups with the oxygens at the ends; three equivalent configurations in either mineral are possible (at 0 GPa, $d(\text{O–H}) = 1.007$ and 0.975 Å, for pe and pvk , respectively). The MSWA-scheme leads to H atoms forming hydroxyls with oxygens in the octahedron where Al replaces Mg in pe ; such O–H groups point to the vacant site. The replacement of Si with Al and the introduction of H in pvk results in the formation of a hydroxyl between a hydrogen and an oxygen of the octahedron hosting the cation substitution, with H taking position inside an adjoining 12-fold Mg-coordinated cage. Six

Table 3
 a and ω parameters for MSWV and MSWA models. See text for their meaning.

ω_0 (kJ/mol)	ω_1 (kJ/mol/GPa)	ω_2 (kJ/mol/GPa 2)
MSWV model		
145411.184	−4.77619218	0.0190667
a_0 (kJ/mol)	a_1 (kJ/mol/GPa)	a_2 (kJ/mol/GPa 2)
-290293	5.7369	0.0057
MSWA model		
ω_0 (kJ/mol)	ω_1 (kJ/mol/GPa)	ω_2 (kJ/mol/GPa 2)
581384	−14.2968	0.0464
a_0 (kJ/mol)	a_1 (kJ/mol/GPa)	a_2 (kJ/mol/GPa 2)
-290293	5.7369	0.0057

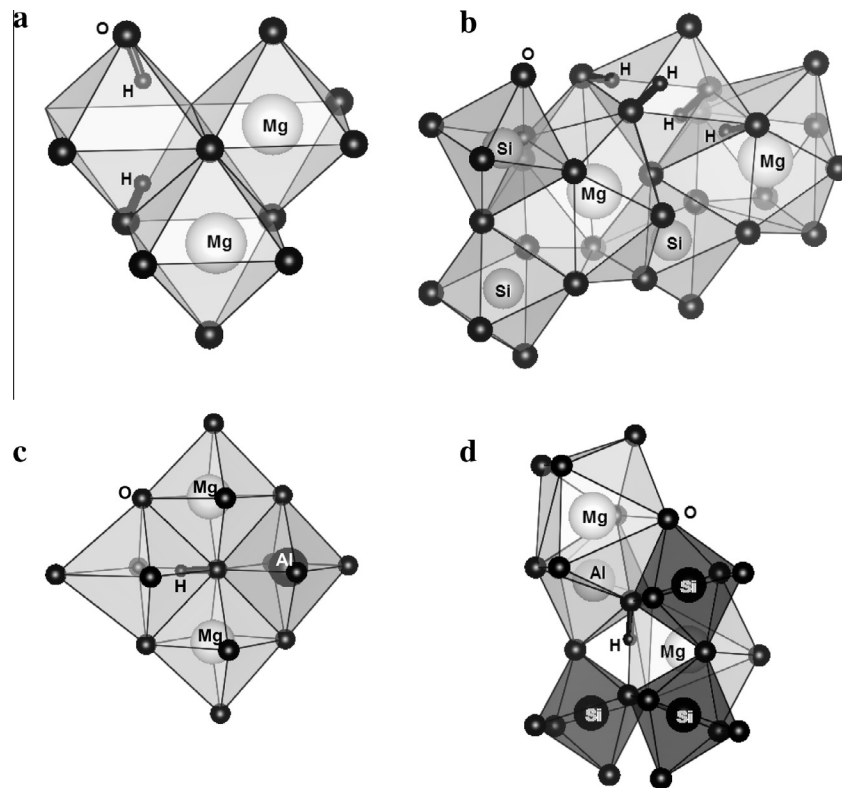


Fig. 1. MSWV H-incorporation model ($Mg^{2+} \leftrightarrow 2H^+$ and $Si^{4+} \leftrightarrow 4H^+$) for periclase (a) and perovskite (b). MSWA H-incorporation model ($2Mg^{2+} \leftrightarrow Al^{3+} + H^+$ and $Si^{4+} \leftrightarrow Al^{3+} + H^+$) for periclase (c) and perovskite (d). See text for further explanation.

possible equivalent arrangements are possible (at 0 GPa, $d(O-H) = 1.029$ and 1.013 \AA , for *pe* and *pvk*, respectively).

For brevity, $L(pe_x)$ and $R(pvk_x)$ are indicated as the left-hand and right-hand member of Eqs. (3) and (4), respectively. A shift in the H-exchange reaction towards $L(pe_x)$ or $R(pvk_x)$, is qualitatively associated to a hydrogen “preference” for entering periclase or perovskite compared to the other phase. Fig. 2a and b, show isothermal $K(P,T,x)$ surfaces determined by either model using Eq. (6.a) at $T = 1500$ and 2500 K (spanning the T -interval derived by plausible geotherms), as a function of pressure and x . The latter ranges up to the largest H_2O -uptake compatible with 1 *pe* mole and 2 *pvk* moles, i.e. $x \approx 0.02$, assuming a 1500 ppm reference bulk water content. It can be observed that MSWV and MSWA lead to two different types of behaviour in H_2O -partitioning mechanisms, although both models give $K(P,T,x)$ figures which are smaller than unity, thus suggesting a shift in the exchange reaction towards $R(pvk_x)$. Such discrepancies are attributed to the $(\xi''_0 + \xi_\omega)$ -functions of Eq. (10). In particular: (i) $(\xi''_0 + \xi_\omega)$ depends on P only, and $\Delta G_0(P,T,x)$ is weakly dependent on T via configuration entropy; (ii) MSWV and MSWA provide $(\xi''_0 + \xi_\omega)$ -figures ranging from 247 to 252, and from 774 and 942 kJ/mol, respectively, over the 10–80 GPa interval. MSWA is therefore expected to show more marked sensitivity to temperature and pressure than MSWV. An intrinsic difference in the two incorporation models is displayed in Fig. 3 via the ξ_ω/ξ''_0 -ratio. Note

that H-uptake mechanisms and “pure” *pe/pvk* behaviour, respectively, are reflected in ξ''_0 and ξ_ω . MSWV seems more prone to the cation substitution scheme than MSVA. Moreover, ξ_ω/ξ''_0 is exhibited as having dissimilar trends as a function of P , which, nevertheless, agree and display decreasing ξ_ω/ξ''_0 -figures upon increasing pressure beyond 45 GPa.

MSWV and MSWA show remarkable dependence on H_2O -uptake, which leads to a general decrease in the equilibrium constant upon increasing x . For example, MSWV gives a $K(P,T,x)$ -variation of 36/25%, between 0 and 0.02 at 1500/2500 K and 80 GPa, compared to 77/60% in MSWA. The temperature affects the $K(P,T,x)$ surface in terms of a shift towards unity at higher T -values. Such behaviour is consistent with the statement that, the higher the temperature, the more the reaction model tends to predict comparable inclinations of *pe* and *pvk* in hosting hydrogen. “Low” T -values bring to light intrinsic differences between MSWV and MSWA incorporation mechanisms, yielding $K(P,T,x)$ s which increasingly diverge from one to another. At $x = 0.02$ and $P = 80 \text{ GPa}$, MSWV and MSWA lead to $K(P,T,x)$ -variations, passing from 1500 to 2500 K, of 16 and 58%, respectively. At $x = 0.02$ and $T = 1500/2500 \text{ K}$, MSWV and MSWA predict changes in the equilibrium constant, from 24 to 80 GPa, of about 2–3 and 17–28%, respectively.

To sum up, this points to H-incorporation energetics being dependent on the replacement mechanism for hosting

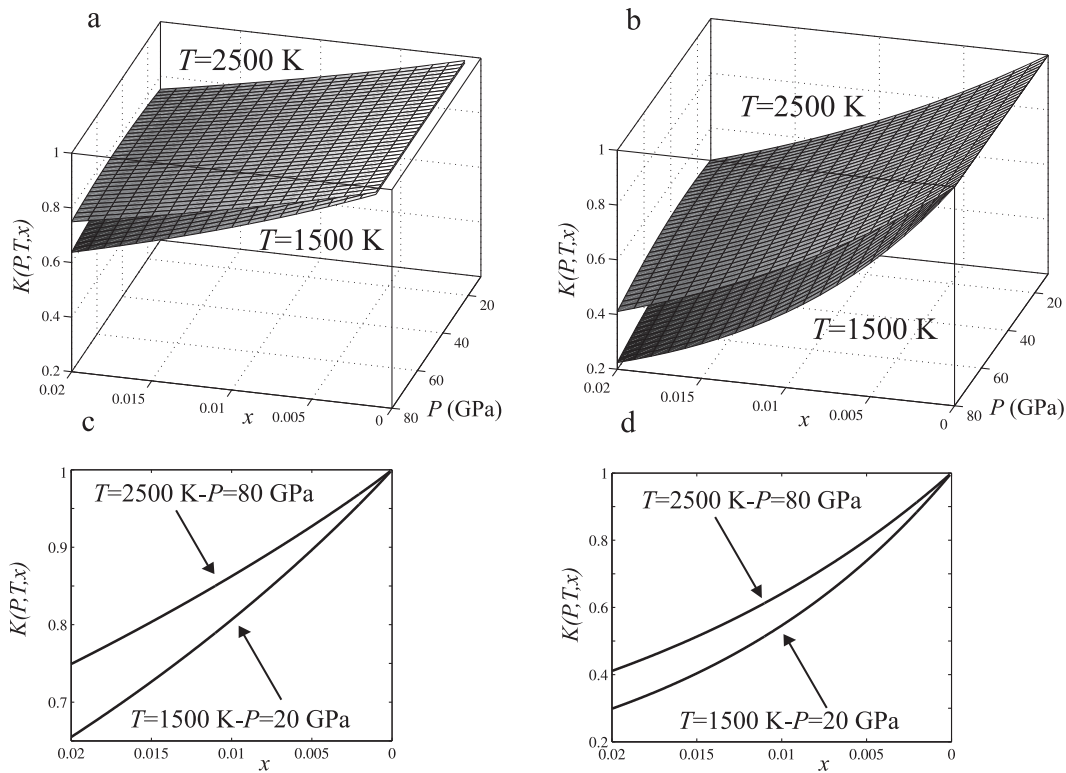


Fig. 2. Equilibrium constant, $K(P, T, x)$, at 1500 and 2500 K, for MSWV (a) and MSWA (b); (c) and (d) show $K(P, T, x)$ as function of x at $P-T$ end values of plausible lower mantle geotherms. From the Eqs. (11.a) and (11.b) of the text, the $P-T$ range explored is 24–80 GPa and $T = 1800\text{--}2600\text{ K}$.

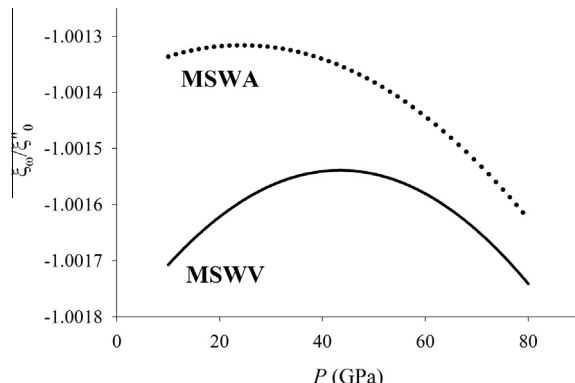


Fig. 3. MSWV, $\xi_{\omega,\text{MSWV}}/\xi''_{0,\text{MSWV}}$, and MSWA, $\xi_{\omega,\text{MSWA}}/\xi''_{0,\text{MSWA}}$, energy modelling. See Eqs. (9.a) and (9.b), for an explanation of ξ s, and Table 3 for the calculations.

hydrogen. Hence, other atomic substitution schemes might shed further light on how far such an uptake reaction is affected by the chemical species involved.

8. DISCUSSION

8.1. Equilibrium constant: MSWV vs MSWA

On the basis of some experimental studies, Fe-free periclase seems to accommodate almost no water in its structure (Bolfan-Casanova et al., 2000, 2002); conversely,

other authors (Murakami et al., 2002; Litasov and Ohtani, 2007) assign high water incorporation capability to this phase, with H_2O -uptake ranging between 0.1 and 0.2 wt% (1000–2000 ppm). Such discrepancies might mirror the main H incorporation mechanisms in the structure of the samples, their being out of $P-T$ thermodynamic equilibrium and/or an analytical strategy for water measurement. Different techniques, i.e. infra-red spectroscopy (Bolfan-Casanova et al., 2000, 2002) versus secondary ion mass spectroscopy (i.e. Inoue et al., 2010), may well yield values which are internally consistent but discrepant with each other (Hernández et al., 2013).

The bulk water content was re-calculated for the *pe-pvk* system in view of the geochemical models in use. Eqs. (3) and (4) require slightly different lower/upper *BWC*-values for the lower mantle: BSE (MSWA, 865/1614 ppm); LM (MSWA, 854/1593 ppm); BSE (MSWV, 869/1629 ppm); LM (MSWV, 859/1608 ppm). Assuming an adiabatic temperature gradient in the lower mantle, ∇T depends on the geochemical model and mineralogical composition (Turcotte and Schbert, 1982; Matas et al., 2007; Murakami et al., 2012). BSE and LM, which imply different convection mechanisms, yield ∇T throughout the investigated P range as large as 0.3 and 0.5 K/km, respectively, in agreement with Ono (2008); therefore, the ensuing $P-T$ relationships used in this study are:

$$T(\text{LM}) = 11.290 \times P + 1648 \quad (11.\text{a})$$

and

$$T(\text{BSE}) = 6.596 \times P + 1686, \quad (11.b)$$

P in GPa and T in K.

An “average equilibrium constant” was introduced, as defined by the equation below

$${}_{BWC}K(P, T) = \frac{1}{BWC} \int_0^{BWC} K(P, T, x) dx \quad (12)$$

where integration is calculated over possible H_2O -uptake values, i.e. x from 0.0, namely a fully anhydrous $pe + pvk$ system, to BWC ($\approx 0.01/0.02$ M H_2O content, according to Fig. 2a and b). The reference notations “1500” and “800” ppm are used to refer to maximum and minimum geochemically sound bulk water content, respectively, instead of its precise values being actually adopted for calculations. The dispersion of the “average equilibrium constant” can then be estimated upon the x -range explored as:

$$\sigma(P, T) = \sqrt{\frac{1}{BWC} \int_0^{BWC} [K(P, T, x) - {}_{BWC}K(P, T)]^2 dx}. \quad (13)$$

In such a case, the notation ${}_{BWC}K(P, T) \pm \sigma(P, T)$ which is expressed below bears no relation to the conventional notion of experimental uncertainty, although Eq. (13) would formally seem to be a standard deviation.

The MSWV partitioning mechanism predicts (Fig. 4a) ${}_{BWC}K(P, T)$ as decreasing upon increasing BWC , indicating a decrease in the H_2O -uptake capacity of pe , and a consequent shift in the exchange reaction towards pvk . Pressure is of negligible effect over the range explored, as proven by very close ${}_{BWC}K(P, T)$ values at 24 GPa and 80 GPa, for both 800 and 1500 BWC ; the most relevant effects are due to temperature. $\sigma(P, T)/{}_{BWC}K(P, T) < 0.1$ suggests moderate dispersion. The difference between BSE and LM, in terms of pe versus pvk contents ($pe/pvk: 0.21$ vs 0.18), is probably too small to bring to light differences in $pe-pvk$ H_2O -uptake capacity when observing the MSWV partitioning mechanism.

MSWA shows similar features (Fig. 4b), but the differences between isobaric-curves and between BWC s are more marked than for MSWV. Different BSE and LM pe/pvk modal proportions are revealed, though ${}_{BWC}K(P, T)$ values

are only modestly influenced in the MSWA exchange mechanism. $\sigma(P, T)/{}_{BWC}K(P, T) < 0.25$ is significantly larger than in MSWV, as a consequence of a quicker changing average equilibrium constant provided by MSWA. Notwithstanding that, the general behaviour of ${}_{BWC}K(P, T)$ is unequivocally determined; no inversion in the H-exchange reaction between pe and pvk is predicted to take place over the explored $P-T$ interval.

Both MSWV and MSWA show weakly varying ${}_{BWC}K(P, T)$ -figures over the P -range of geochemical interest ($P = 24-80$ GPa). The LM-model ($T = 1920-2564$ K; Eq. (11.a)) leads to an H-exchange equilibrium constant with the following values at the geotherm upper and lower ends: $0.835/0.905(\pm 0.088/\pm 0.052)-0.858/0.919(\pm 0.076/\pm 0.044)$, for MSWV and 1500/800 ppm, and $0.624/0.770(\pm 0.184/\pm 0.121)-0.646/0.785(\pm 0.175/\pm 0.114)$, for MSWA and 1500/800 ppm. In turn, BSE ($T = 1846-2222$ K; Eq. (11.b)) gives ${}_{BWC}K(P, T)$ at the geotherm upper and lower ends of $0.830/0.902(\pm 0.090/\pm 0.053)-0.842/0.910(\pm 0.084/\pm 0.049)$, for MSWV and 1500/800 ppm, and $0.614/0.762(\pm 0.188/\pm 0.125)-0.607/0.757(\pm 0.190/\pm 0.127)$, for MSWA and 1500/800 ppm (Fig. 4).

Narrow ${}_{BWC}K(P, T)$ ranges suggest the introduction of a “grand average” of ${}_{BWC}K(P, T)$ calculated along each explored $P-T$ geotherm (Eqs. (11.a) and (11.b)), namely

$$\langle {}_{BWC}K \rangle = \frac{1}{\Delta P} \int_{P_0}^{P_{max}} {}_{BWC}K(P, T(P)) dP. \quad (14)$$

In so doing, it is plausible to consider that $\langle {}_{BWC}K \rangle$ efficiently provides an overall description of the equilibrium constant for H-exchange reactions as a function of BWC only.

BSE and LM provide $\langle {}_{BWC}K \rangle$ s close to one another, for a given incorporation scheme and BWC value (Table 4). $\langle {}_{BWC}K \rangle$ shows relevant sensitivity to BWC and, overall, the H-exchange mechanism. On the basis of the $\langle {}_{BWC}K \rangle$ s in Table 4, the $d(\langle {}_{BWC}K \rangle)/d(BWC)$ slopes can be determined; these are weakly dependent on the geochemical model and significantly sensitive to the microscopic reaction mechanism, thus obtaining -0.00003 , for MSWA, and -0.00001 ppm⁻¹, for MSWV.

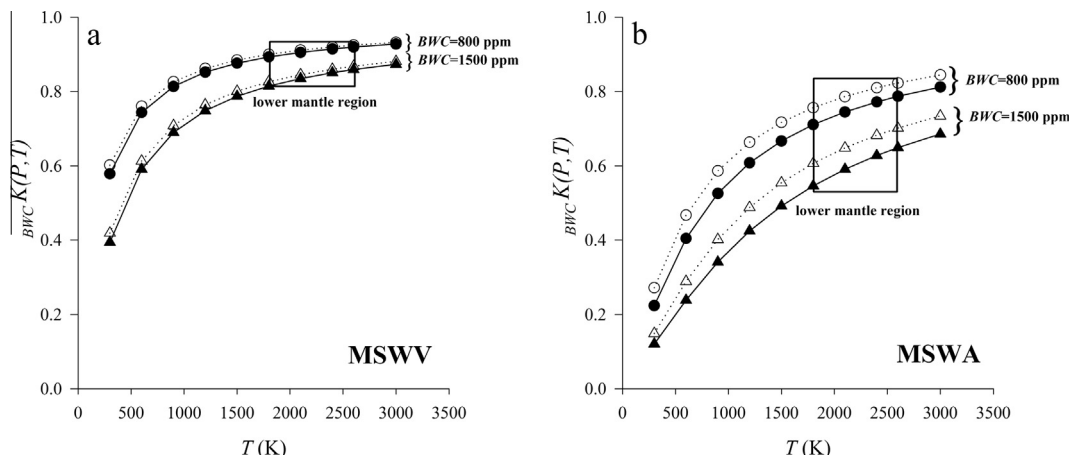


Fig. 4. ${}_{BWC}K(P, T)$ as a function of P , T and BWC (Bulk Water Content), for MSWV (a) and MSWA (b). Empty and filled symbols correspond to 24 and 80 GPa, respectively. Triangles: H_2O uptake value of ≈ 1500 ppm; circles: H_2O uptake value of ≈ 800 ppm.

In summary, the pe/pvk H-exchange equilibrium constant of the MSWV mechanism may ultimately be considered as a constant value of ≈ 0.875 in the $P-T$ interval of interest ($\approx 24\text{--}80$ GPa, 1800–2600 K) and with a bulk water content over the reference range. Such a figure is the mean of $\langle_{BWC}K\rangle$ -values in Table 4 for LM and BSE. Conversely, in the MSWA mechanism, $\langle_{BWC}K\rangle$ is more sensitive to BWC (and LM over BSE), but its values still lie in a rather narrow range, namely 0.61–0.78.

8.2. H_2O concentration-based partition coefficient ($Kd_{H_2O}^{pe/pvk}$)

The perovskite + periclase + H_2O system can be described as anhydrous-periclase + anhydrous-perovskite + H-bearing-periclase + H-bearing-perovskite, to the extent that equilibrium is provided by an H-exchange (x), according to reactions (3) and (4). Considering that H_2O -content is comparatively very low and assuming activity coefficients equal to unity, then

$$\langle_{BWC}K\rangle \approx \left[\left(\frac{\lambda_{pvk}}{\lambda_{pvk_H}} \right)^2 \left(\frac{\lambda_{pe_H}}{\lambda_{pe}} \right) \right],$$

where: λ_A is the fraction molar content related to the A -phase; pvk_H and pe_H refer to general H-bearing perovskite and periclase, respectively; note that $_H$ is not to be confused with $_x$, the latter indicating precise x - H_2O content in the exchange equilibrium reaction. By assuming that fully anhydrous phases occur in negligible amounts, and therefore λ_{pvk_H} and λ_{pe_H} are the sole significant terms stemming from the equilibrium reactions ($\lambda_{pvk_H} + \lambda_{pe_H} = 1$), then the above equation could be simplified to

$$\langle_{BWC}K\rangle \approx \frac{\lambda_{pe_H}}{(1 - \lambda_{pe_H})^2} \quad (14.a)$$

Table 4

$\langle_{BWC}K\rangle$, average of the equilibrium reaction constant over the lower mantle $P-T$ range (24–80 GPa and 1800–2600 K), as a function of Bulk Water Content, BWC (ppm), for the two H-incorporation models (MSWV and MSWA). Bold: BWC reference values of geochemical interest.

BWC (ppm)	$\langle_{BWC}K\rangle$ BSE model	$\langle_{BWC}K\rangle$ LM model
MSWV		
100	0.987	0.988
300	0.962	0.965
800	0.906	0.913
1500	0.836	0.848
2000	0.791	0.806
2500	0.749	0.767
3000	0.711	0.731
MSWA		
100	0.965	0.968
300	0.899	0.908
800	0.759	0.780
1500	0.610	0.638
2000	0.529	0.559
2500	0.462	0.494
3000	0.408	0.439

On the other hand, if anhydrous phases dominate the bulk of the system, and hydrous terms may be treated as a sub-system to the extent that $\lambda_{pvk_H} + \lambda_{pe_H} = 1$ is still valid, then the equilibrium equation would become

$$\langle_{BWC}K\rangle \approx \frac{\lambda_{pe_H}}{(1 - \lambda_{pe_H})^2} \cdot 4, \quad (14.b)$$

where factor 4 accounts for 2 pvk -moles *versus* 1 pe -mole of quasi-anhydrous material.

The ratio between H_2O -contents hosted by periclase and perovskite (i.e. $C_{H_2O}^{pe}/C_{H_2O}^{pvk}$) can be estimated using Eq. (14.a) and (14.b) and $\langle_{BWC}K\rangle$ values. $C_{H_2O}^{pe}/C_{H_2O}^{pvk}$ (formally named “partition coefficient”: $Kd_{H_2O}^{pe/pvk}$) is therefore a useful instrument for directly comparing these results with experimental data.

Fig. 5a displays $Kd_{H_2O}^{pe/pvk}$ trends as a function of BWC , determined by Eq. (14.a) for the LM and BSE models using the $\langle_{BWC}K\rangle$ in Table 4. Irrespective of the geochemical model, MSWV and MSWA give the same concentration ratio over the two phases ($Kd_{H_2O}^{pe/pvk} \approx 0.6$) at “low to very low” bulk water content ($BWC < 500$ ppm). Upon

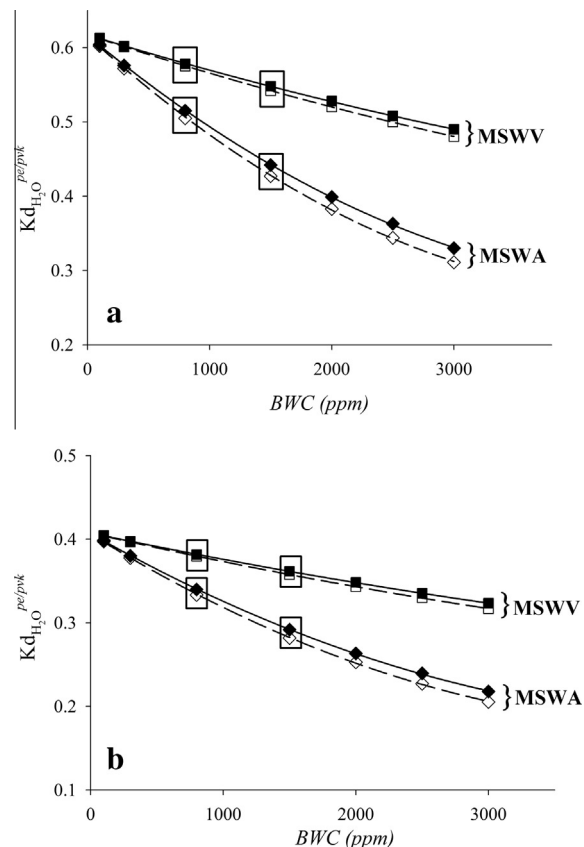


Fig. 5. Periclase-to-perovskite H_2O -contents ratio ($Kd_{H_2O}^{pe/pvk}$) as a function of BWC . (a) $Kd_{H_2O}^{pe/pvk}$ values obtained by Eq. (14.a); (b) $Kd_{H_2O}^{pe/pvk}$ values obtained by Eq. (14.b). LM-MSWV: filled squares/filled line; LM-MSWA: filled diamonds/filled line; BSE-MSWV: empty squares/dashed line; BSE-MSWA: empty diamonds/dashed line. LM and BSE are referred to Layered Mantle and Bulk Silicate Earth geochemical models respectively.

increasing the potential bulk water content, $Kd_{H_2O}^{pe/pvk}$ decreases, exhibiting divergent trends as a function of the exchange mechanism. In particular, it can be observed that the MSWV-linear interpolation slope is close to 0 ($Kd_{H_2O}^{pe/pvk} = 0.60 - 0.49$; BWC spanning from 500 to 3000 ppm). In the light of this, a $Kd_{H_2O}^{pe/pvk}$ of 0.56 can be assumed for MSWV.

MSWA, in turn, leads to a $Kd_{H_2O}^{pe/pvk}$ -trend with a slightly steeper negative slope, which yields ≈ 0.3 $Kd_{H_2O}^{pe/pvk}$, for a potential (possibly unrealistic) 3000 ppm bulk water content. MSWA- $Kd_{H_2O}^{pe/pvk}$ may also be considered nearly invariant and as high as 0.47 in the 800–1500 ppm region when obtained as the average over the 0.43–0.51 interval.

Fig. 5b, in turn, provides $Kd_{H_2O}^{pe/pvk}$ from Eq. (14.b). In this case, a decrease in $Kd_{H_2O}^{pe/pvk}$ by an average ≈ 0.65 factor takes place compared to the values predicted by Eq. (14.a).

Combining MSWV and MSWA results (Fig. 5a and b) leads to the proposal that $Kd_{H_2O}^{pe/pvk}$ lies in the 0.31–0.56 interval, over the $P-T-BWC$ range of interest (≈ 24 –80 GPa, 1800–2600 K, 800–1500 ppm), suggesting pe hosting H_2O in terms of 248–840 ppm.

These results are compared to those by Hernández et al. (2013), who used a different computing frame and hypothesised H-incorporation at the expense of Mg for both pe and pvk , obtaining a pe/pvk partition coefficient value of ≈ 0.01 . This mechanism was also tested here. However, since it was too time-consuming to replicate the original calculations and beyond the main aims of the present study, we restricted our investigation to H-sites in the pvk 12-fold coordination Mg-vacated cage, which were close to corner-oxygen atoms, without exploring how a change in super-cell size can affect the hydrogen position. This restriction implies that the resulting $Kd_{H_2O}^{pe/pvk}$ values do not have the same degree of accuracy as for the MSWV and MSWA models, but they are of the same order of magnitude. $Kd_{H_2O}^{pe/pvk}$ resulted in values of ≈ 0.37 –0.60 over the $P-T-BWC$ interval of interest, in line with MSWV and MSWA attainments. Such comparisons lead to a conclusion which confirms the tendency of perovskite to be a better repository phase for water than periclase in the lower mantle, on the basis of the most likely potential incorporation mechanisms despite the variance in values obtained. Such discrepancies might be reflective of the different approaches to extract $Kd_{H_2O}^{pe/pvk}$: in the present case $Kd_{H_2O}^{pe/pvk}$ relies upon exploitation of the grand-average equilibrium reaction constant, whereas in the case explored by Hernández et al. (2013) it is determined upon Gibbs energy minimization.

Moreover, experimental $Kd_{H_2O}^{pe/pvk}$ values span a disquieting range of 0.2–75 (Bolfan-Casanova et al., 2000; Murakami et al., 2002, 2002; Litasov et al., 2003; Ohtani, 2005; Inoue et al., 2010). This could be explained by relevant experimental difficulties both in performing hydrous experiments at extreme pressures and temperatures and in analysing small H_2O concentrations in the resulting tiny crystals (Keppler and Smyth, 2006 and reference therein).

In conclusion, the results point out that the macroscopic behaviour of $H_2O^{pe/pvk}$ partitioning may reflect microscopic H incorporation mechanisms, which take place locally, and that both pvk and pe act as potential repository phases for water, the former showing almost double the water storage capacity of the latter in the lower mantle.

9. CONCLUSIONS

On the basis of two different H-incorporation mechanisms and two geochemical lower mantle models, calculated $BWC K(P,T)$ values lie in the ≈ 0.6 – ≈ 0.9 range, showing that H-exchange reactions shift towards pvk , independently of the microscopic H-uptake scheme, i.e. MSWV or MSWA. However, MSWV and MSWA H-incorporation models lead to dissimilar trends, the latter giving smaller equilibrium constant values and showing more marked sensitivity to $P-T$ than the former. Both microscopic models give $BWC K(P,T)$ which decreases with an increase in bulk water contents (BWC), suggesting an increase of penchant in pvk to host water. In general, MSWV and MSWA exhibit a modest, quasi-negligible, dependence on P , whereas both are sensitive to temperature and in particular to BWC . It is worth noting that $BWC K(P,T)$ varies little over the $P-T$ range predicted by LM and BSE geochemical frames for the lower mantle, and can therefore be replaced by its average ($\langle BWC K \rangle$) calculated over the pressure–temperature path forecast using geochemical models. Regardless of the microscopic H-exchange reaction, LM and BSE models lead to $\langle BWC K \rangle$ ranging from 0.638 to 0.913, and from 0.610 to 0.906, respectively.

To summarise, the equilibrium constant of the H-incorporation reactions exhibits complex dependence on natural environment variables (P , T , BWC) and microscopic mechanisms. If pe and pvk are considered to occur in the lower mantle as H-bearing phases, then H_2O is distributed according to various possible partitioning mechanisms, including those for MSWV and MSWA, which were investigated in the present study. MSWV and MSWA lead to different equilibrium constant values, whose discrepancies become apparent, in particular in the case of $K(P,T,x)$. This suggests that the microscopic uptake scheme greatly affects the equilibrium constant.

The experimentally determined H_2O partitioning pe/pvk spans the extremely wide 0.2–75 range. Such a large interval might reflect the following: (i) thermodynamic meta-equilibrium in experiments, compared to ideal cases used in the calculations; (ii) as a consequence of (i), defects (cation replacements and deviations from ideal crystal structure), which widely occur in specimens from HP-HT synthesis, remarkably change the capacity of hosting hydrogen in a phase.

On the basis of the developed model, it was therefore proposed that the partition coefficient, $Kd_{H_2O}^{pe/pvk}$, lies in the narrow interval 0.31–0.56 by combining the results for MSWV and MSWA in the $P-T-BWC$ range of interest (≈ 24 –80 GPa, 1800–2600 K, 800–1500 ppm). This implies that (i) both pvk and pe act as potential repository phases for water, the former showing almost double the water storage capacity of the latter in the lower mantle and

(ii) even at low or very low bulk water content, periclase hardly ever becomes a pure anhydrous phase.

ACKNOWLEDGEMENTS

This study was supported by MIUR-2010EARRZ_003 Grant (A.P.) and PNRA_2013 B02.02 (C.B.). The authors are grateful to D. Belmonte and two anonymous reviewers for their constructive criticism. M. Toplis and the Senior Editor are acknowledged for their useful remarks and comments, which helped to significantly improve the quality of the manuscript.

REFERENCES

- Abe Y., Ohtani E., Okuchi T., Righter K. and Drake M. (2000) Water in the early Earth. In *Origin of the Earth and Moon* (eds. R. M. Canup and K. Righter). University of Arizona Press, Tucson, pp. 413–433.
- Ahrens T. J. (1989) Water storage in the mantle. *Nature* **342**, 122–123.
- Anderson O. L. (1989) Composition of the Earth. *Science* **243**, 367–370.
- Anderson O. L. (1998) Thermoelastic properties of MgSiO₃ perovskite using the Debye approach. *Am. Mineral.* **83**, 23–35.
- Belmonte D., Ottanello G. and Vetuschi Zuccolini. M. (2013) Melting of α -Al₂O₃ and vitrification of the undercooled alumina liquid: ab initio vibrational calculations and their thermodynamic implications. *J. Chem. Phys.* **138**, 064507. <http://dx.doi.org/10.1063/1.479061>.
- Belmonte D., Ottanello G. and Vetuschi Zuccolini. M. (2014) Ab initio thermodynamic and thermophysical properties of sapphirine end-members in the join Mg₄Al₈Si₂O₂₀–Mg₃Al₁₀SiO₂₀. *Am. Mineral.* **99**, 1449–1461.
- Bolfan-Casanova N. (2005) Water in the Earth's mantle. *Min. Mag.* **69**, 229–257.
- Bolfan-Casanova N., Keppler H. and Rubie D. C. (2000) Partitioning of water between mantle phases in the system MgO–SiO₂–H₂O up to 24 GPa: implications for the distribution of water in the Earth's mantle. *Earth Planet. Sci. Lett.* **182**, 209–221.
- Bolfan-Casanova N., Mackwell S., Keppler H., McCammon C. and Rubie D. C. (2002) Pressure dependence of H solubility in magnesiowüstite up to 25 GPa: implications for the storage of water in the Earth's lower mantle. *Geophys. Res. Lett.* **29**(10), 1029–1032.
- Bolfan-Casanova N., McCammon C. A. and Mackwell S. J. (2006) Water in transition zone and lower mantle minerals. In *Earth's Deep Water Cycle* (eds. S. D Jacobsen and S. Van Der Lee) Geophysical Monograph Series, vol. 168AGU. doi: <http://dx.doi.org/10.1029/168GM06>.
- Bonadiman C., Hao Y., Coltorti M., Dallai L., Huang U. and Xia Q. (2009) Water contents of pyroxenes in intraplate lithospheric mantle. *Eur. J. Mineral.* **21**, 637–647.
- Cammarano F. and Romanowicz B. (2007) Insights into the nature of the transition zone from physically constrained inversion of long period seismic data. *PNAS-High Pressure Geosci.* **104**, 9139–9144.
- Cappellini G., Bouquette-Russo S., Amadon B., Noguera C. and Finocchi F. (2000) Structural properties and quasiparticle energies of cubic SrO, MgO and SrTiO₃. *J. Phys.: Condens. Matter* **12**, 3671–3688.
- Causà M., Dovesi R., Pisani C. and Roetti C. (1986) Electronic structure and stability of different crystal phases of magnesium oxide. *Phys. Rev. B* **33**, 1308–1316.
- Corgne A., Liebske C., Wood B. J., Rubie D. C. and Frost D. J. (2005) Silicate perovskite–melt partitioning of trace elements and geochemical signature of a deep perovskitic reservoir. *Geochim. Cosmochim. Acta* **69**, 485–496.
- Dai L. and Karato S. (2009) Electrical conductivity of wadsleyite at high temperatures and high pressures. *Earth Planet. Sci. Lett.* **287**, 277–283.
- Demouchy S., Mackwell S. J. and Kohlstedt D. L. (2007) Influence of hydrogen on Fe–Mg interdiffusion in (Mg, Fe)O and implications for Earth's lower mantle. *Contrib. Mineral. Petrol.* **154**, 279–289.
- Dixon J. E., Leist L., Langmuir C. and Schilling J. G. (2002) Recycled dehydrated lithosphere observed in plume-influenced mid-ocean-ridge basalt. *Nature* **420**, 385–389.
- Dovesi, Saunders V. R., Roetti C., Orlando R., Zicovich-Wilson C. M., Pascale F., Civalleri B., Doll K., Harrison N. M., Bush I. J., D'Arco P. and Llunell M. (2009) *CRYSTAL09 User's Manual*. University of Torino, Italy.
- Fiquet G., Andrault D., Dewaele A., Charpin T., Kunz M. and Häusermann D. (1998) P–V–T equation of state of MgSiO₃. *Phys. Earth Planet. Inter.* **105**, 21–31.
- Gale J. D. (1997) GULP: a computer program for the symmetry-adapted simulation of solids. *J. Chem. Soc. Faraday Trans.* **93**, 629–637.
- Garnero E. J., Maupin V., Lay T. and Fouch M. J. (2004) Variable azimuthal anisotropy in Earth's lowermost mantle. *Science* **306**, 259–261.
- Ghosh S., Ohtani E., Litasov K. D., Suzuki A., Dobson D. and Funakoshi K. (2013) Effect of water in depleted mantle on post-spinel transition and implication for 660 km seismic discontinuity. *J. Chem. Soc. Sci. Lett.* **371**, 103–111.
- Griffin J. M., Berry J. A., Frost D. J., Wimperis S. and Ashbrook S. E. (2013) Water in the Earth's mantle: a solid-state NMR study of hydrous wadsleyite. *Chem. Sci.* **4**, 1523–1538.
- Guyot F., Madon M., Peyronneau J. and Poirier J. P. (1988) X-ray microanalysis of high-pressure/high-temperature phases synthesized from natural olivine in a diamond anvil cell. *Earth Planet. Sci. Lett.* **90**, 52–64.
- Hauri E. H., Gaetani G. A. and Green T. H. (2006) Partitioning of water during melting of the Earth's upper mantle at H₂O-undersaturated conditions. *Earth Planet. Sci. Lett.* **248**, 715–734.
- Hernández E. R., Alfè D. and Brodholt J. (2013) The incorporation of water into lower mantle perovskites: a first-principles study. *Earth Planet. Sci. Lett.* **364**, 37–43.
- van der Hilst R. D., Widjiantoro S. and Engdahl E. R. (1997) Evidence for deep mantle circulation from global tomography. *Nature* **386**, 578–584.
- Hirschmann M. M. (2006) Water, melting, and the deep Earth H₂O cycle. *Ann. Rev. Earth Planet. Sci.* **34**, 629–653. <http://dx.doi.org/10.1146/annurev.earth.34.031405.125211>.
- Hirschmann M. M. and Kohlstedt D. (2012) Water in Earth's mantle. *Phys. Today* **65**(3), 40–45.
- Hirschmann M. M., Aubaud C. and Withers A. C. (2005) Storage capacity of H₂O in nominally anhydrous minerals in the upper mantle. *Earth Planet. Sci. Lett.* **236**, 167–181. <http://dx.doi.org/10.1016/j.epsl.2005.04.022>.
- Hirschmann M. M., Tenner T., Aubaud C. and Withers A. C. (2009) Dehydration melting of nominally anhydrous mantle: the primacy of partitioning. *Phys. Earth Planet. Inter.* **176**, 54–68.
- Huang X., Xu Y. and Karato S. (2005) Water content in the transition zone from electrical conductivity of wadsleyite and ringwoodite. *Nature* **434**, 746–749.
- Ingrin J. and Skogby H. (2000) Hydrogen in nominally anhydrous upper mantle minerals: concentration levels and implications. *Eur. J. Mineral.* **12**, 543–570.

- Inoue T. (1994) Effect of water on melting phase relations and melt composition in the system Mg_2SiO_4 – $MgSiO_3$ – H_2O up to 15 GPa. *Phys. Earth Planet. Inter.* **85**, 237–263.
- Inoue T., Wada T., Sasaki R. and Yurimoto H. (2010) Water partitioning in the Earth's mantle. *Phys. Earth Planet. Inter.* **183**, 245–251.
- Irfune T. (1994) Absence of an aluminous phase in the upper part of the Earth's lower mantle. *Nature* **370**, 131–133.
- Irfune T., Koizumi T. and Ando J. (1996) An experimental study of the garnet-perovskite transformation in the system $MgSiO_3$ – $Mg_3Al_2Si_3O_{12}$. *Geophys. Res. Lett.* **96**, 147–157.
- Ito E. and Takahashi E. (1989) Postspinel transformations in the system Mg_2SiO_4 – Fe_2SiO_4 and some geophysical implications. *J. Geophys. Res.* **94**(B8), 10637.
- Ito E., Kubo A., Katsura T. and Walter M. J. (2004) Melting experiments of mantle materials under lower mantle conditions with implications for magma ocean differentiation. *Phys. Earth Planet. Inter.* **143**–**144**, 397–406.
- Jahn S., Rahner R., Dachs E., Mrosko M. and Koch-Müller M. (2013) Thermodynamic properties of anhydrous and hydrous wadsleyite, β - Mg_2SiO_4 . *High Pressure Res.* **33**, 584–594.
- Javoy M., Kaminski E., Guyot F., Andrault D., Sanlou J. R., Moreira M., Labrosse S., Jambon A., Agrinier P., Davaille A. and Jaupart C. (2010) The chemical composition of the Earth: enstatite chondrite models. *Earth Planet. Sci. Lett.* **293**, 259–268.
- Joachim B., Wohlers A., Norberg N., Gardés E., Petrishcheva E. and Abart R. (2013) Diffusion and solubility of hydrogen and water in periclase. *Phys. Chem. Miner.* **40**, 19–27.
- Johnson E. A. (2006) Water in nominally anhydrous crustal minerals: speciation, concentration and geological significance. In *Reviews in Mineralogy and Geochemistry*, vol. 62 (eds. J. Smyth and H. Keppler). Mineralogical Society of America, pp. 117–154.
- Karato S. and Jung H. (2003) Effects of pressure on high-temperature dislocation creep in olivine polycrystals. *Philos. Mag. A* **83**, 401–414.
- Kellogg L. H., Hager B. H. and van der Hilst R. D. (1999) Compositional stratification in the deep mantle. *Science* **283**, 1881–1884.
- Keppler H. and Bolfan-Casanova N. (2006) Thermodynamics of water solubility and partitioning. In: Water in nominally anhydrous minerals. In *Reviews in Mineralogy and Geochemistry*, vol. 62 (eds. J. Smyth and H. Keppler). Mineralogical Society of America, pp. 193–230.
- Kesson S. E., Fitz Gerald J. D., Shelley J. M. G. and Withers R. L. (1995) Phase relations, structure and crystal chemistry of some aluminous silicate perovskites. *Earth Planet. Sci. Lett.* **134**, 187–201.
- Khan A. and Shankland T. J. (2012) A geophysical perspective on mantle water content and melting: inverting electromagnetic sounding data using laboratory-based electrical conductivity profiles. *Earth Planet. Sci. Lett.* **317**–**318**, 27–43.
- Kleppe A. K. (2006) High-pressure Raman spectroscopic studies of hydrous wadsleyite II. *Am. Mineral.* **91**, 1102–1109.
- Kröger F. A. (1972) *The Chemistry of Imperfect Crystals*. North-Holland, Amsterdam, 1039 p.
- Lay T., Williams Q. and Garnero E. J. (1998) The core–mantle boundary layer and deep Earth dynamics. *Nature* **392**, 461–468.
- Lay T., Garnero E. J. and Williams Q. (2004) Partial melting in a thermo-chemical boundary layer at the base of the mantle. *Phys. Earth Planet. Inter.* **146**, 441–467.
- Lee C., Yang W. and Parr R. G. (1988) Development of the Colle-Salvetti correlation-energy formula into a functional of the electron density. *Phys. Rev. B* **37**, 785–789.
- Li J. and Agee C. B. (1996) Geochemistry of mantle–core differentiation at high pressure. *Nature* **381**, 686–689.
- Lin J. F. and Wheat A. (2012) Electronic spin transition of iron in the Earth's lower mantle. *Hyperfine Interact.* **207**, 81–88.
- Litasov K. D. (2010) The influence of Al_2O_3 on the H_2O content in periclase and ferropericlase at 25 GPa. *Russ. Geol. Geophys.* **51**, 644–649.
- Litasov K. D. and Ohtani E. (2007) Effect of water on the phase relations in Earth's mantle and deep water cycle. In *Advances in High-pressure Mineralogy* (ed. E. Ohtani). Geological Society of America, pp. 115–156.
- Litasov K. D., Ohtani E., Langenhorst F., Yurimoto H., Kubo T. and Kondo T. (2003) Water solubility in Mg-perovskites, and water storage capacity in the lower mantle. *Earth Planet. Sci. Lett.* **211**, 189–203.
- Litton D. A. and Stephen Garofalini S. H. (2001) Modeling of hydrophilic wafer bonding by molecular dynamics simulations. *J. Appl. Phys.* **89**, 6013–6023.
- Lyubetskaya T. and Korenaga J. (2007) Chemical composition of Earth's primitive mantle and its variance. I. method and results. *J. Geophys. Res.* **112**, B03211. <http://dx.doi.org/10.1029/2005JB004223>.
- Mackwell S. J., Bystricky M. and Sproni C. (2005) Fe–Mg interdiffusion in (Mg, Fe)O. *Phys. Chem. Miner.* **32**, 418–425.
- Mao W. L., H-k Mao., Sturhahn W., Zhao J., Prakapenka V. B., Yue Meng Y., Shu J., Fei Y. and Hemley R. J. (2006) Iron-rich post-perovskite and the origin of ultralow-velocity zones. *Science* **312**, 564–565.
- Marty B. (2012) The origins and concentrations of water, carbon, nitrogen and noble gases on Earth. *Earth Planet. Sci. Lett.* **313**–**314**, 56–66.
- Matas J., Bass J., Ricard Y., Mattern E. and Bukowinski M. S. T. (2007) On the bulk composition of the lower mantle: predictions and limitations from generalized inversion of radial seismic profiles. *Geophys. J. Int.* **170**, 764–780.
- McCammon C. E., Stachel T. and Harris J. W. (2004) Iron oxidation state in lower mantle mineral assemblages II. Inclusions in diamonds from Kankan, Guinea. *Earth Planet. Sci. Lett.* **222**, 423–434.
- McDonough W. F. and Arevalo R. (2008) Uncertainties in the composition of Earth, its core and silicate sphere. *J. Phys. – Conf. Ser.* **136** 022006 (abstr).
- McDonough W. F. and Sun S. (1995) The composition of the Earth. *Chem. Geol.* **120**, 223–253.
- Mei S. and Kohlstedt D. L. (2000) Influence of water on plastic deformation of olivine aggregates: 2 Dislocation creep regime. *J. Geophys. Res.* **105**, 21471–21481.
- Merli M., Sciascia L., Pavese A. and Diella V. (2015) Modelling of thermo-chemical properties over the sub-solidus MgO – FeO binary, as a function of iron spin configuration, composition and temperature. *Phys. Chem. Miner.* **42**, 347–362.
- Michael P. J. (1988) The concentration, behavior and storage of H_2O in the suboceanic upper mantle – implications for mantle metasomatism. *Geochim. Cosmochim. Acta* **52**, 555–566.
- Montelli R., Nolet G., Masters G., Engdahl E. R. and Hung S.-H. (2004) Finite-frequency tomography reveals a variety of plumes in the mantle. *Science* **303**, 338–343.
- Mosenfelder J. L., Sharp T. G., Asimow P. D. and Rossman G. R. (2013) Hydrogen Incorporation in natural mantle olivines. In *Earth's Deep Water Cycle* (eds. S. D. Jacobsen and S. Van Der Lee). American Geophysical Union, Washington, D.C. <http://dx.doi.org/10.1029/168GM05>.
- Murakami M., Hirose K., Yurimoto H., Nakashima S. and Takafuji N. (2002) Water in Earth's lower mantle. *Science* **295**, 1885. <http://dx.doi.org/10.1126/science.1065998>.

- Murakami M., Ohishi Y., Hirao N. and Hirose K. (2012) A perovskitic lower mantle inferred from high-pressure, high-temperature sound velocity data. *Nature* **485**, 90–94.
- Nomura R., Hirose K., Uesugi K., Ohishi Y., Tsuchiyama A., Miyake A. and Ueno Y. (2014) Low core-mantle boundary temperature inferred from the solidus of pyrolite. *Science* **343**, 522–525.
- Oganov A. R. and Brodholt J. P. (2000) High-pressure phases in the Al_2SiO_5 system: the problem of aluminous phase in the Earth's lower mantle: *ab initio* calculations. *Phys. Chem. Miner.* **27**, 430–439.
- Ohira I., Ohtani E., Sakai T., Miyahara M., Hirao N., Ohishi Y. and Nishijima M. (2014) Stability of a hydrous δ -phase, $\text{ALOOH}-\text{MgSiO}_2(\text{OH})_2$, and a mechanism for water transport into the base of lower mantle. *Earth Planet. Sci. Lett.* **401**, 12–17.
- Ohtani E. (2005) Effect of water on phase transitions in the Earth's mantle. *Elements* **1**, 25–30.
- Ono S. (2008) Experimental constraints on the temperature profile in the lower mantle. *Phys. Earth Planet. Inter.* **170**, 267–273.
- Otsuka K., McCammon C. A. and Karato S.-I. (2010) Tetrahedral occupancy of ferric iron in $(\text{Mg}, \text{Fe})\text{O}$: implications for point defects in the Earth's lower mantle. *Phys. Earth Planet. Inter.* **180**, 179–188.
- Ottanello G., Civalleri B., Ganguly J., Vetuschi Zuccolini M. and Noel Y. (2008) Thermo-physical properties of the a–b–c polymorphs of Mg_2SiO_4 : an all-electron *ab initio* study. *Phys. Chem. Miner.* **36**, 87–106.
- Palme H. and O'Neill H. St. C. (2003) Cosmochemical estimates of Mantle Composition. In *Treatise on Geochemistry*, vol. 2 (eds. H. D. Holland and K. K. Turrekian). Elsevier, Amsterdam, The Netherlands, pp. 1–38.
- Pamato M. G., Myhill R., Boffa Ballaran T., Frost D. J., Heidelbach F. and Miyajima N. (2015) Lower mantle water reservoir implied by the extreme stability of a hydrous aluminosilicate. *Nat. Geosci.* **8**, 75–79.
- Panero W. R. and Stixrude L. (2004) Hydrogen incorporation in stishovite at high pressure and symmetric hydrogen bonding in d- ALOOH . *Earth Planet. Sci. Lett.* **221**, 421–431.
- Panero W. R., Pigott J. S., Reaman D. M., Kabbes J. E. and Liu Z. (2015) Dry $(\text{Mg}, \text{Fe})\text{SiO}_3$ perovskite in the Earth's lower mantle. *J. Geophys. Res. Solid Earth* **120**, 894–908.
- Parisi F., Sciascia L., Princivalle F. and Merli M. (2012) The pressure induced ringwoodite to Mg-perovskite and periclase post-spinel phase transition: a Bader's topological analysis of the ab initio electron densities. *Phys. Chem. Miner.* **39**, 103–113.
- Pearson D. G., Brenker F. E., Nestola F., McNeill J., Nasdala L., Hutchinson M. T., Matveev S., Mather K., Slversmit G., Schmitz S., Vekemans B. and Vincze L. (2014) Hydrous mantle transition zone indicated by ringwoodite included within diamond. *Nature* **507**, 221–224.
- Ringwood A. E. (1991) Phase transitions and their bearing on the constitution and dynamics of the mantle. *Geochim. Cosmochim. Acta* **55**, 2083–2110.
- Saal A. E., Hauri E., Langmuir C. H. and Perfit M. R. (2002) Vapour undersaturation in primitive mid-ocean-ridge basalt and the volatile content of Earth's upper mantle. *Nature* **419**, 451–455.
- Salter V. J. M. and Stracke A. (2004) Composition of the depleted mantle. *Geochem. Geophys. Geosyst.* **5**, 27. <http://dx.doi.org/10.1029/2003GC000597>.
- Saxena S. K., Liermann H.-P. and Shen G. (2004) Formation of iron hydride and high-magnetite at high pressure and temperature. *Phys. Earth Planet. Inter.* **146**, 313–317.
- Scanavino I. and Prencipe M. (2013) Ab-initio determination of high-pressure and high-temperature thermoelastic and thermodynamic properties of low-spin $(\text{Mg}_{1-x}\text{Fe}_x)\text{O}$ ferropericlase with x in the range [0.06, 0.59]. *Am. Mineral.* **98**, 1270–1278.
- Scanavino I., Belousov R. and Prencipe M. (2012) Ab initio quantum-mechanical study of the effects of the inclusion of iron on thermoelastic and thermodynamic properties of periclase (MgO). *Phys. Chem. Miner.* **39**, 649–663.
- Smyth J. R. (1994) A crystallographic model for hydrous wadsleyite: an ocean the Earth's interior? *Am. Mineral.* **79**, 1021–1025.
- Smyth J. R. and Jacobsen S. D. (2006) Nominally anhydrous minerals and Earth's deep water cycle. In *Earth's Deep Water Cycle*, vol. 168 (eds. S. D. Jacobsen and S. van der Lee). American Geophysical Union, pp. 1–11.
- Smyth J. R. (2006) Hydrogen in high pressure silicate and oxide mineral structures. In *Water in nominally anhydrous minerals*, vol. 62 (eds. J. Smyth and H. Keppler). Geochemical Society-Mineralogical Society of America, pp. 85–115.
- Stacey F. D. and Isaak D. G. (2003) Anharmonicity in mineral physics: a physical Interpretation. *J. Geophys. Res.* **108(B9)**, 2440.
- Stashans A., Eras L. and Chamba G. (2009) Modelling of Al impurity in perovskite and ilmenite structures of MgSiO_3 . *Phys. Chem. Miner.* **37**, 191–199.
- Stixrude L. and Bukowinski M. S. T. (1992) Stability of $(\text{Mg}, \text{Fe})\text{SiO}_3$ perovskite and the structure of the lowermost mantle. *Geophys. Res. Lett.* **19**, 1057–1060.
- Stixrude L., Lithgow-Bertelloni C., Kiefer B. and Fumagalli P. (2007) Phase stability and shear softening in CaSiO_3 perovskite at high pressure. *Phys. Rev. B* **75**, 024108.
- Trønnes R. G. and Frost D. J. (2002) Peridotite melting and mineral-melt partitioning of major and minor elements at 21–24 GPa. *Earth Planet. Sci. Lett.* **197**, 117–131.
- Turcotte D. L. and Schubert G. (1982) *Geodynamics*. Wiley, New York, pp. 456.
- Valerio G., Catti M., Dovesi R. and Orlando R. (1995) Ab initio study of antiferromagnetic rutile-type FeF_2 . *Phys. Rev. B* **52**, 2422–2427.
- Van Orman J. A., Li C. and Crispin K. L. (2009) Aluminum diffusion and Al-vacancy association in periclase. *Phys. Earth Planet. Inter.* **172**, 34–42.
- Walter M. J., Nakamura E., Trønnes R. G. and Frost D. J. (2004) Experimental constraints on crystallization differentiation in a deep magma ocean. *Geochim. Cosmochim. Acta* **68**, 4267–4284.
- Wentzcovitch R. M., Yu Y. G. and Wu Z. (2010) Thermo-dynamic Properties and Phase Relations in Mantle Minerals Investigated by First Principles Quasiharmonic Theory. In *Theoretical and Computational Methods in Mineral Physics: Geophysical Applications*, vol. 71 (eds. R. Wentzcovitch and L. Stixrude). Reviews in Mineralogy and Geochemistry, p. 59.
- Williams Q. and Hamley R. J. (2001) Hydrogen in the deep Earth. *Annu. Rev. Earth Planet. Sci.* **29**, 365–418.
- Wolfe C. J., Solomon S. C., Laske G., Collins J. A., Detrick R. S., Orcutt J. A., Bercovici D. and Hauri E. H. (2009) Mantle shear-wave velocity structure beneath the Hawaiian hot spot. *Science* **326**, 1388–1390.
- Wood B. J. and Corgne A. (2007) Trace elements and hydrogen in the Earth's transition zone and lower mantle. In *Mineral Physics*, vol. 2 (ed. G. D. Price) (ed. G. Schubert). Elsevier, Amsterdam, pp. 63–89.

- Wu Z. and Cohen R. E. (2006) More accurate generalized gradient approximation for solids. *Phys. Rev. B* **73**, 235116.
- Wysession M. E., Lay T., Revenaugh J., Williams Q., Garnero E., Jeanloz R., and Kellogg L. (1998) The D'' discontinuity and its implications. In The Core-Mantle Boundary Region (eds. M.Gurnis, M. E. Wysession, E. Knittl and Buffet B.) Geodyn. SerAGU, Washington, D.C., vol. 28, pp. 273–297.
- Zhao Y. and Donald Truhlar D. G. (2009) Calculation of semiconductor band gaps with the M06-L density functional. *J. Chem. Phys.* **130**, 074103–074105.
- Zindler A. and Hart S. (1986) Chemical geodynamics. *Annu. Rev. Earth Planet. Sci.* **14**, 493–571.

Associate editor: Michael J. Toplis